†Work sponsored by the Department of the Air Force.
*Part of this work was performed at the Francis Bitter National Magnet Laboratory, M.I.T.

[1]A review of narrow-gap semiconductor infrared lasers is given by T. C. Harman, in Proceedings of the Conference on the Physics of Semimetals and Narrow Gap Semiconductors, Dallas, 1970 (unpublished); J. Phys. Chem. Solids Suppl. (to be published).

[2]A review of the lead-tin chalcogenides, their preparation, properties, and applications as detectors is given by Ivars Melngailis and T. C. Harman, in *Semiconductors and Semimetals*, edited by R. K. Willardson and A. C. Beer (Academic, New York, 1970), Vol. VII.

[3]J. R. Burke, J. D. Jensen, and B. Houston, Ref. 1.

[4]John Melngailis, J. A. Kafalas, and T. C. Harman, Ref. 1.

[5]G. A. Antcliffe, R. T. Bate, and J. S. Wrobel, Bull. Am. Phys. Soc. 14, 330 (1969).

[6]John Melngailis, T. C. Harman, J. G. Mavroides, and J. O. Dimmock, Bull. Am. Phys. Soc. 14, 330 (1969).

[7]M. K. Norr, J. Electrochem. Soc. 109, 433 (1962).

[8]L. A. Roth and P. N. Argyres, in *Semiconductors and Semimetals*, edited by R. K. Willardson and A. C. Beer (Academic, New York, 1966), Vol. I, p. 185.

[9]R. Kubo, S. J. Miyake, and N. Hashitsume, in *Solid State Physics*, edited by F. Seitz and D. Turnbull (Academic, New York, 1965), Vol. 17, p. 361; A. H. Kahn and H. P. R. Fredrikse, *ibid.*, Vol. 9.

[10]I. M. Lifshitz and A. M. Kosevich, Zh. Eksperim. i Teor. Fiz. 29, 730 (1955) [Soviet Phys. JETP 2, 636 (1956)]; J. Phys. Chem. Solids 4, 1 (1958).

[11]P. T. Panousis, Ph.D. thesis, Iowa State University, 1967 (unpublished). The main subroutines and instruction on their use were kindly provided by H. A. Ashworth of Carnegie-Mellon University.

[12]J. R. Burke, B. Houston, and H. T. Savage, Phys. Rev. B 2, 1977 (1970).

[13]J. R. Burke, B. Houston, H. T. Savage, J. Babiskin, and P. G. Liebermann, J. Phys. Soc. (Dunod, Paris, 1964), 384 (1966).

[14]K. F. Cuff, M. R. Ellett, C. D. Kuglin, and L. R. Williams, in *Proceedings of International Conference on the Physics of Semiconductors* (Dunod, Paris, 1964), p. 677.

[15]W. Schilz, J. Phys. Chem. Solids 30, 893 (1969).

[16]C. K. N. Patel and R. E. Slusher, Phys. Rev. 177, 1200 (1969).

[17]J. F. Butler and A. R. Calawa, in *Physics of Quantum Electronics*, edited by P. L. Kelley, B. Lax, and P. E. Tannenwald (McGraw-Hill, New York, 1966), pp. 458–466.

[18]J. F. Butler, Solid State Commun. 7, 909 (1969).

[19]J. O. Dimmock, Ref. 1.

[20]J. F. Butler and T. C. Harman, IEEE J. Quantum Electron. QE5, 50 (1969); Ivars Melngailis and A. R. Calawa, Appl. Phys. Letters 9, 304 (1966).

PHYSICAL REVIEW B VOLUME 3, NUMBER 2 15 JANUARY 1971

Infrared Absorption in *p*-Type GaP

J. D. Wiley and M. DiDomenico, Jr.
Bell Telephone Laboratories, Murray Hill, New Jersey 07974
(Received 1 September 1970)

Infrared absorption measurements have been performed on Zn-doped GaP at 300 and 90 °K. The absorption observed at 300 °K between 1 and 12 μ is attributed to a combination of intraband free-carrier absorption (FCA) and direct interband absorption arising from transitions between the Γ_8 and Γ_7 (splitoff) valence bands. The absorption at 90 °K is identified as photoionization of holes from the Zn acceptor levels to the Γ_8 and Γ_7 valence bands. Because of the small spin-orbit splitting (82 meV) and strong nonparabolicity of the valence bands in GaP, both the interband and intraband absorption are qualitatively different from similar absorption in other III-V compounds. The interband transitions give rise to extremely broad overlapping absorption bands while the FCA exhibits an unusually large magnitude. We propose a model for FCA in *p*-GaP which includes the effect of virtual intermediate states in the light-hole and splitoff valence bands. It is shown, on the basis of this model, that FCA in *p*-GaP should have a wavelength dependence which depends on the scattering mechanism in the usual way, but whose magnitude is enhanced by the additional intermediate states. In agreement with transport measurements, we find that holes are scattered principally by acoustic and nonpolar optical phonons.

I. INTRODUCTION

Infrared absorption has proved to be an extremely valuable tool in the study of energy band structures, lattice vibrations, and scattering mechanisms in semiconductors.[1] In the case of GaAs, for example, infrared absorption has yielded important information about the conduction[2–4] and valence-band structures,[5,6] lattice vibrational modes,[7,8] and the scattering mechanisms for free carriers.[9–11] Similar success has been obtained in infrared studies of the $GaAs_{1-x}P_x$ alloy system[12–15] and of *n*-type GaP.[16–20] The case of *p*-type GaP, however, is complicated by the unusually small spin-orbit split-

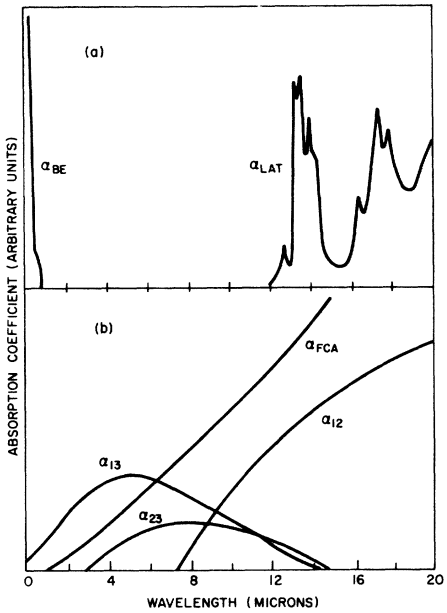

FIG. 1. Schematic summary of the wavelength ranges in which various intrinsic (a) and extrinsic (b) absorption processes are expected to occur in p-GaP at 300 °K. The intrinsic processes are the fundamental band-edge absorption α_{BE}, and lattice absorption α_{LAT}. The extrinsic mechanisms are intraband free-carrier absorption α_{FCA}, and direct intervalence-band absorption α_{12}, α_{13}, and α_{23} (see Fig. 3 for valence-band nomenclature).

ting,[21] $\Delta_0 \approx 82 \pm 1$ meV, which separates the Γ_8 and Γ_7 (splitoff) valence bands at $k = 0$. Because Δ_0 is small, much of the absorption due to direct intervalence-band transitions occurs in a region of the infrared where lattice absorption and intraband free-carrier absorption (FCA) are strong. Furthermore, the close proximity of the Γ_7 and Γ_8 valence bands requires a substantial modification of the usual expression for FCA and, as we shall show, results in an enhanced intraband absorption for carriers in the Γ_8 valence band.

Figure 1 shows in schematic form a summary of the various intrinsic [Fig. 1(a)] and extrinsic [Fig. 1(b)] absorption processes which are expected to occur in p-type GaP at 300 °K. In undoped material the absorption is negligibly small from the band edge (2.26 eV or $\lambda = 0.55$ μ) to $\lambda \approx 12$–18 μ, where two-phonon lattice absorption gives rise to a series of strong absorption peaks.[22,23] The main reststrahlen bands occur in the region $\lambda = 25$–28 μ and cause extinction of the transmitted radiation for $24 < \lambda < 30$ μ. In p-type material the free holes can give rise to direct intervalence-band absorption[1,24,25] and phonon-assisted intraband absorption[26–30] (FCA). The latter process gives rise to the Drude-like background labeled α_{FCA} in Fig. 1(b). The intervalence-band absorption shown schematically in Fig. 1(b) is, of course, dependent upon the details of the valence-band structure near $k = 0$ and will be discussed in Sec. II.

As the temperature of the sample is lowered, the FCA and interband absorption, which are proportional to the free-hole concentration, decrease as the holes become frozen to Zn acceptors. Nevertheless, the infrared absorption *increases* monotonically as the temperature is lowered and is considerably greater at 90 °K than it was at 300 °K. This is attributed to photoionization of holes from Zn acceptors to the valence bands. The photoionization absorption is directly proportional to the density of neutral acceptors and hence increases as the temperature decreases. The total extrinsic absorption at any temperature is therefore

$$\alpha_{total} = (1-f)\alpha_{PI} + f(\alpha_{FCA} + \alpha_{IB}), \quad (1)$$

where f is the fraction of uncompensated acceptors which are ionized, and the subscripts PI, FCA, and IB denote photoionization, intraband free-carrier absorption, and interband absorption, respectively. Whether the total absorption is an increasing or decreasing function of temperature depends on the strength of α_{PI} compared to α_{IB} and α_{FCA}.

Section II contains the experimental results of absorption measurements at 300 °K and a discussion of possible explanations for the rather unusual magnitude and wavelength dependence of this absorption. In Sec. III, we present the results of low-temperature absorption measurements and identify the source of this absorption as photoionization of Zn acceptors.

II. ABSORPTION AT 300°K

A. Experimental

The Zn-doped GaP crystals used in this study were grown from Ga solution at 1170 °C and were partially compensated with oxygen by the addition of 0.02-mole% Ga_2O_3 to the melt. Thin single-crystal samples with faces perpendicular to a [111] direction were mechanically polished with 0.1-μ diamond paste. The net acceptor (Zn) concentrations were measured by surface-barrier capacitance techniques and are listed in Table I together with calculated hole concentrations at 300 °K and sample thicknesses. In calculating the hole concentrations we have assumed a donor (oxygen) concentration[31] of 8×10^{16} cm^{-3} and Zn ionization energies[32] of 60, 46, and 34 meV for samples B, C, and D. Expressions given by Blakemore[33] were then used to compute p.

The experimental apparatus was standard, utilizing a globar source, a Leiss double monochrometer with KBr prisms, and a Golay cell detector. The light was chopped at 13 Hz and synchronously detected. Transmission ratios were measured as a function of wavelength by a sample-in/sample-out

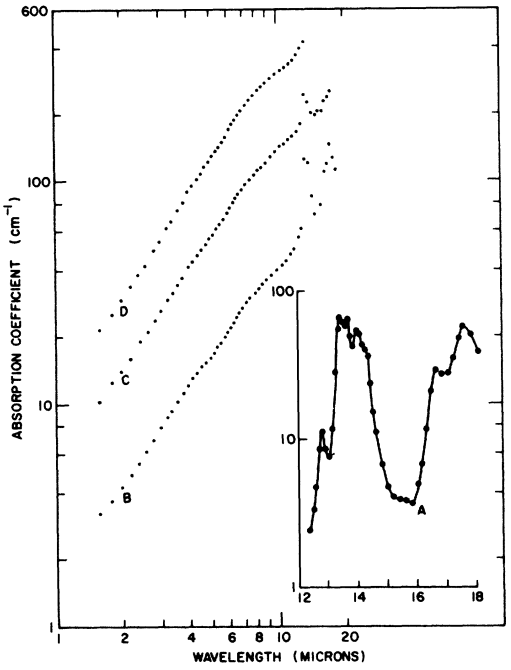

FIG. 2. Experimental absorption data for the samples listed in Table I. The absorption for sample A (undoped) was <1 cm^{-1} for $\lambda<12$ μ.

technique and absorption coefficients were calculated from transmission ratios in the usual manner.[34] For wavelengths below 4 μ the reflection coefficient was calculated using the refractive-index measurements of Bond.[35] At longer wavelengths, where the influence of lattice absorption becomes important, the index of refraction was calculated using an expression given by Barker.[23] The resulting reflectivity ranged from 0.267 at $\lambda=1$ μ to 0.200 at $\lambda=20$ μ.

The experimental absorption coefficients are shown in Fig. 2. Strong lattice absorption begins at $\lambda\approx 12$ μ with a series of two-phonon peaks which have been previously identified.[22,23] Below 12 μ the absorption in the undoped sample A was too low to measure accurately but had an upper limit of $\alpha\lesssim 2$ cm^{-1}. Recent measurements[36] on thicker samples have shown that the three-phonon and higher-order processes contribute less than 1 cm^{-1} of absorption. The absorption observed at 300 °K in the doped crystals (B, C, and D) is relatively featureless and, to within experimental error, scales linearly with both Zn concentration and calculated hole concentration.

The monotonically increasing absorption observed in p-GaP is in striking contrast with the rich and informative absorption spectra observed in p-type Ge,[1,24,25] GaAs,[5,6] and AlSb.[5] In fact, from a comparison of Fig. 2 with the schematic absorption shown in Fig. 1(b), it would appear that the absorption in p-GaP is composed mainly of FCA. There is some small reproducible structure in the form of slope changes at $\lambda\approx 4$ μ and 7–8 μ but, as can be seen from Fig. 2, the over-all appearance is that of a strong Drude-like background absorption with a wavelength dependence of λ^p where $p\approx 1.6$–1.7. This wavelength dependence is suggestive of intraband FCA in the presence of acoustic and nonpolar optical-mode scattering.[27,28] We have recently shown[37] that these are precisely the scattering mechanisms that appear to be dominant in the p-type III–V compounds. If FCA is indeed the predominant source of absorption the *magnitude* of the absorption is considerably greater than predicted by conventional theories of FCA. The simple Drude model, for example, gives an absorption coefficient which, for p-GaP at 300 °K, can be written as

$$\alpha/N=1.75\times10^{-17}\lambda^2/\mu\ , \qquad (2)$$

where α/N is the absorption cross section in cm^2, λ is the wavelength in microns, and μ is the mobility in cm^2/V sec. Using a mobility[32] of 90 cm^2/V sec for sample B leads to a predicted absorption coefficient of 0.04 cm^{-1} at $\lambda=1$ μ and 4 cm^{-1} at $\lambda=10$ μ. These values are to be compared with observed absorption coefficients of 2 and 40 cm^{-1} at 1 and 10 μ, respectively. Similar difficulties are encountered in attempting to explain the magnitude using existing quantum theories of FCA. The absorption at 10 μ is approximately 50 times greater than predicted for pure acoustic-mode scattering[27,28] if one uses the 5.7-eV valence-band deformation potential determined from transport measurements.[37]

Thus it appears that the observed absorption is either a rather fortuitous combination of intervalence-band absorptions which happens to yield a monotonic wavelength dependence, or an anomalously strong intraband FCA. We now discuss these pos-

TABLE I. Zn-doped GaP crystals used in infrared absorption studies.

Sample	Zn conc.[a] (cm^{-3})	Hole density p(300 °K)[b] (cm^{-3})	Thickness[c] of samples (mm)
A	undoped		0.378
B	$2\pm0.2\times10^{17}$	$1.6\pm0.2\times10^{17}$	2.02, 0.388
C	$5\pm0.3\times10^{17}$	$3.6\pm0.2\times10^{17}$	0.09, 0.192
D	$1.1\pm0.3\times10^{18}$	$6.4\pm0.2\times10^{17}$	0.0625, 0.157

[a]Net acceptor concentration measured by surface-barrier capacitance. Error bars correspond to variation within and among samples.

[b]Calculated free-hole concentration at 300 °K taking account of differing compensation ratios and the variation of the Zn ionization energy with doping level.

[c]When two samples of the same material were used, they agreed in absorption and Zn concentration to within 10%.

sibilities in detail.

B. Direct Intervalence-Band Transitions

The valence-band structure of GaP near $k=0$ is shown in Fig. 3. The v_1 and v_2 bands (heavy- and light-hole bands, respectively) are degenerate at $k=0$ and are separated from the v_3 band by a $k=0$ spin-orbit splitting of $\Delta_0 = 82 \pm 1$ meV.[21] Away from $k=0$ the v_1 and v_2 bands are separated by an amount which depends on $\vec{k}$. In the $\langle 100\rangle$ and $\langle 111\rangle$ directions they become asymptotically parallel as shown in Fig. 3(a) but in all other directions the $v_1 - v_2$ separation increases rapidly with $|\vec{k}|$. Figure 3(b) shows the v_1, v_2, and v_3 bands averaged over all directions in k space. In calculating the bands of Fig. 3 we have used Kane's[25] $\vec{k}\cdot\vec{p}$ secular equation together with the band parameters $L=-8.2$, $M=-2.9$, and $N=-9.0$ (all in units of $\hbar^2/2m_0$, where m_0 is the free-electron mass) as calculated by Faulkner.[38] We are ignoring small effects due to the lack of inversion symmetry in the zinc-blende lattice. The average over all directions was performed by calculating $E(\vec{k})$ along the lines from Γ to X, L, K, U, and W, and then weighting these directions as follows:

$$\langle E_i(k)\rangle = 0.056E_i^X(k) + 0.194E_i^L(k) + 0.194E_i^K(k) + 0.250E_i^W(k) + 0.306E_i^U(k)\ , \qquad (3)$$

where the subscript i is a band index. The weighting factor for a particular set of directions represents the fraction of the total surface area of the Brillouin zone which is closer to those directions than to any others. It should be noted, in passing, that Bowers and Mahan[39] have given a different set of band parameters for GaP [$A=-5.61$, $B=0.11$, and $C^2=13.6$ corresponding to $L=-6.39$, $M=-6.72$, and $N=(-)6.4$ all in units of $\hbar^2/2m_0$]. We have chosen to use Faulkner's values for two reasons. (i) Faulkner used a more extensive basis set (230 plane waves as opposed to 15 used by Bowers and Mahan) for calculating the pseudowave functions which are needed for the evaluation of N, L, and M. (ii) When the parameters of Bowers and Mahan are used to calculate energy bands and hole effective masses, they lead to anomalies such as a near degeneracy of the v_1 and v_2 bands in the $\langle 100\rangle$ directions and $k=0$ effective masses which are considerably lower than the observed masses[32,40] in p-GaP.

For purposes of characterizing the valence bands we can define isotropic effective masses by

$$\langle m_{1,2}^*\rangle = \hbar^2k^2/2\langle E_{1,2}(k)\rangle\ ,$$
$$\langle m_3^*\rangle = \hbar^2k^2/2\,[E_3(k)-\Delta_0]\ , \qquad (4)$$

where, for convenience, we consider $E_i(k)$ and m_i^* to be positive quantities. The effective masses given by Eq. (4) are plotted versus k in Fig. 4. It is seen from Fig. 4 that, except for a very small region near $k=0$, one has $\langle m_1^*\rangle > \langle m_2^*\rangle > \langle m_3^*\rangle$. At 300 °K a thermal population of $E \gtrsim kT \approx 26$ meV in v_1 and v_2 results in holes with k values $\gtrsim 0.05$ and $0.03a_0^{-1}$, respectively. Thus, since the interband transition matrix elements increase[24] with $|k|$, most of the room-temperature interband absorption in p-GaP occurs in a region where $\langle m_1^*\rangle > \langle m_2^*\rangle > \langle m_3^*\rangle$. This is qualitatively different from the situation which prevails in Ge,[6,24,25] GaAs,[5,6] and AlSb.[5] In those materials, the larger spin-orbit splittings lead to a weaker interaction among v_1, v_2, and v_3 in Kane's $\vec{k}\cdot\vec{p}$ Hamiltonian. This, in turn, extends the region of k space over which the $k=0$ masses are valid, and preserves the $k=0$ ordering $\langle m_1^*\rangle > \langle m_3^*\rangle > \langle m_2^*\rangle$ over a larger volume of the thermally populated region near $k=0$. Thus, in the simple parabolic model of Kahn,[24] the $v_1 \rightarrow v_3$ and $v_2 \rightarrow v_3$ absorptions share a common threshold at $\hbar\omega = \Delta_0$, but the $v_1 \rightarrow v_3$ process is restricted to $\hbar\omega > \Delta_0$ while the $v_2 \rightarrow v_3$ process occurs only for $\hbar\omega < \Delta_0$. In contrast, if the Kahn model is applied to GaP, both $v_1 \rightarrow v_3$ and $v_2 \rightarrow v_3$ processes occur for

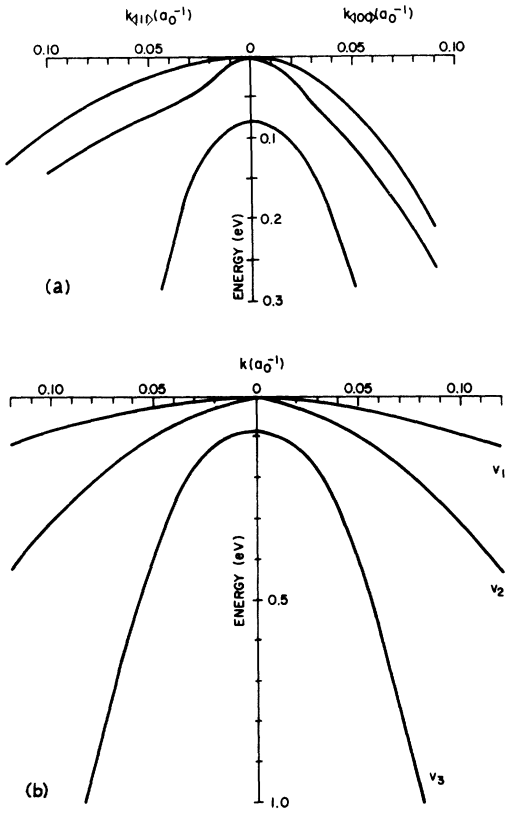

FIG. 3. Valence bands of GaP as calculated for the $\langle 100\rangle$ and $\langle 111\rangle$ directions (a) and averaged over all directions (b). The zone boundary is at $k=0.60a_0^{-1}$ in the $\langle 100\rangle$ directions at $k=0.52a_0^{-1}$ in the $\langle 111\rangle$ directions, where $a_0=0.529$ Å is the Bohr radius.

$\hbar\omega > \Delta_0$. This is shown in Fig. 5, where we have plotted the wavelength dependences of α_{12}, α_{13}, and α_{23} as calculated for GaP using the expressions[24]

$$\frac{\alpha_{12}}{p} = c_{12}\left(\frac{1}{\lambda}\right)^{1/2}\left[\exp\left(-\frac{\beta}{\lambda}\,\frac{\langle m_2^*\rangle}{\langle m_1^*\rangle - \langle m_2^*\rangle}\right) - \exp\left(-\frac{\beta}{\lambda}\,\frac{\langle m_1^*\rangle}{\langle m_1^*\rangle - \langle m_2^*\rangle}\right)\right],$$

$$\frac{\alpha_{13}}{p} = c_{13}\left(\frac{1}{\lambda} - \frac{1}{\lambda_0}\right)^{1/2} \times \exp\left[-\beta\left(\frac{1}{\lambda} - \frac{1}{\lambda_0}\right)\frac{\langle m_3^*\rangle}{\langle m_1^*\rangle - \langle m_3^*\rangle}\right], \tag{5}$$

and

$$\frac{\alpha_{23}}{p} = c_{23}\left(\frac{1}{\lambda} - \frac{1}{\lambda_0}\right)^{1/2} \times \exp\left[-\beta\left(\frac{1}{\lambda} - \frac{1}{\lambda_0}\right)\frac{\langle m_3^*\rangle}{\langle m_2^*\rangle - \langle m_3^*\rangle}\right].$$

In Eq. (5), p is the hole concentration, the c_{ij}'s are coefficients containing material parameters and interband momentum matrix elements, λ is the wavelength, $\lambda_0 = hc/\Delta_0$, and $\beta = hc/kT$. For effective masses we have used $\langle m_1^*\rangle = 1.6$, $\langle m_2^*\rangle = 0.4$, and $\langle m_3^*\rangle = 0.1 m_0$. These values give the best parabolic approximations to the bands of Fig. 3(b) in the sense that they minimize the errors in the *interband energy separations* (not individual band curvatures) for $k \lesssim 0.1 a_0^{-1}$.

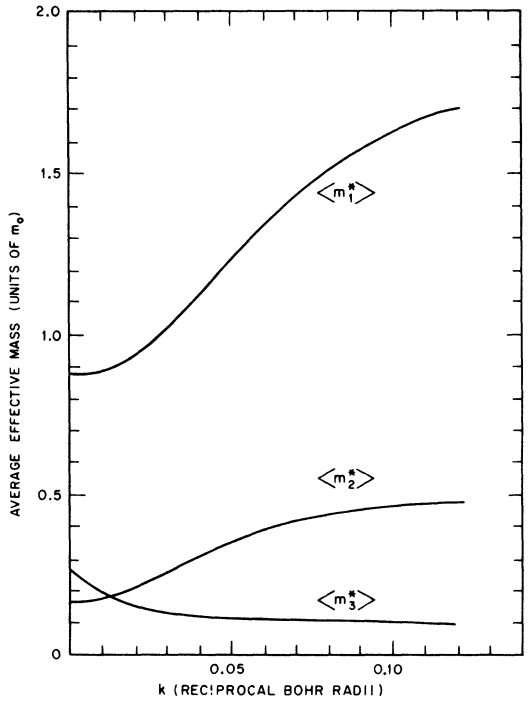

FIG. 4. Averaged valence-band effective masses as defined in Eq. (4). Note that the effective mass of the light-hole band (v_2) is less than that for the split-off band (v_3) only for $k \lesssim 0.01 a_0^{-1}$.

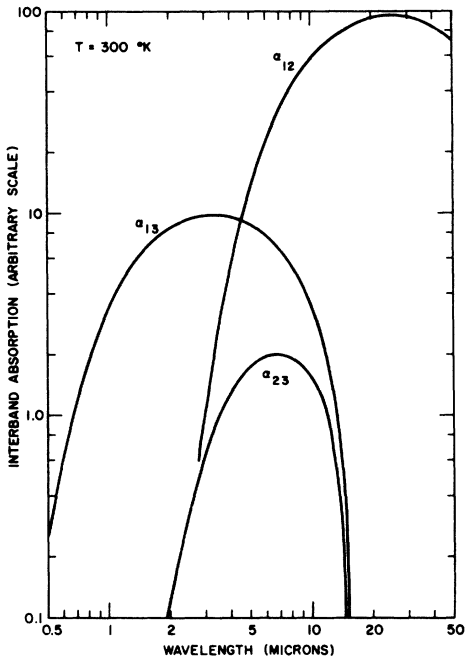

FIG. 5. Wavelength dependence of the direct interband absorption calculated using Eq. (5).

The absorption bands shown in Fig. 5 are only rough approximations of the actual interband absorption. Kane[25] has performed calculations for p-Ge which take account of the nonparabolicity and warping of the bands, and has obtained results which are significantly different from those of Kahn.[24] In particular, the joint density of states for the $v_2 \rightarrow v_3$ absorption has a saddle-point singularity near $k = 0$, where our large-k effective-mass approximation breaks down. This singularity occurs at different k values for different directions and leads to a very complex absorption spectrum in the region $\hbar\omega \lesssim \Delta_0$. Nevertheless, for $1 < \lambda < 10\ \mu$, Fig. 5 is probably realistic.

It is difficult to estimate the magnitudes of the interband absorptions since there have been no calculations of the interband momentum matrix elements for GaP. Judging from the Ge, GaAs, and AlSb results, we would expect the peaks of the absorption bands to obey $\alpha_{12} > \alpha_{13} \gtrsim \alpha_{23}$. The absorption cross section at the peak of α_{13} at 300 °K is $\approx 0.7 \times 10^{-16}$ cm^2 for GaAs,[5,6] and $\approx 0.4 \times 10^{-16}$ cm^2 for AlSb. If the cross section is comparable in GaP we would predict $\alpha_{13} \approx 6$–10 cm^{-1} for sample B at $\lambda = 3.5\ \mu$. This is of the correct magnitude to explain the observed absorption at that wavelength.

Similar arguments can be made concerning the other absorption bands. If, in the absence of more direct knowledge of the matrix elements, the magnitudes of α_{13}, α_{23}, and α_{12}' are arbitrarily adjusted in an attempt to fit the data with interband absorption *alone*, one can obtain a reasonable fit to the data when the peak heights are in the ratio 1:2.5:20. The fit is substantially improved, however, by the addition of a $\lambda^{1.7}$ power-law (FCA) background to the interband absorption as shown in Fig. 6. The relative peak heights for α_{13}, α_{23}, and α_{12} in Fig. 6 are 1:1:9, in good agreement with similar absorption bands in Ge, GaAs, and AlSb. The magnitude of the Drude-like background in Fig. 6 is 15 cm^{-1} at $\lambda = 10$ μ. This is roughly four times the FCA predicted by the Drude theory. It should be noted that the dominant absorption at short wavelengths is α_{13} and that α_{13} has an exponential tail which extends into the visible. Such a tail has been observed[41] in optical absorption in p-GaP for $\lambda < 1$ μ. If the dominant absorption at 1 μ were FCA, one would expect a power-law tail.

In view of the approximate nature of our interband absorption estimates, it is unrealistic to attach too much significance to the fit shown in Fig. 6. Nevertheless, it seems clear that a strong component of FCA is present in the absorption. Since this FCA contribution exceeds conventional theoretical estimates it is appropriate to reexamine the theory of FCA as it applies to p-type semiconductors.

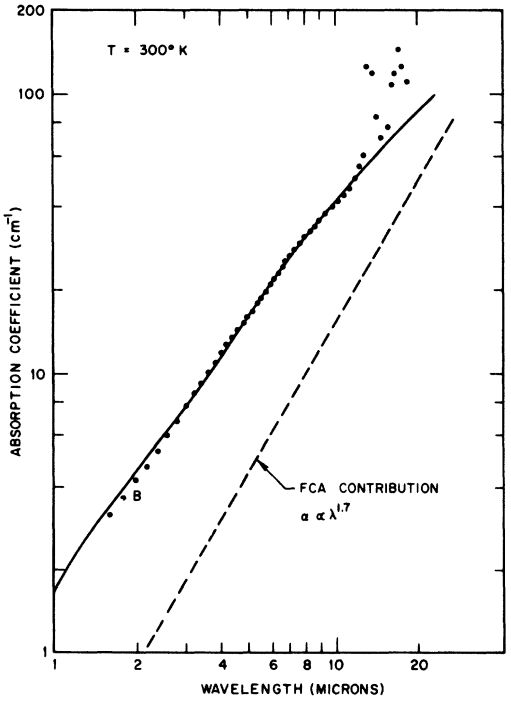

FIG. 6. Illustration of the agreement which can be obtained between the experimental absorption (sample *B*) and a superposition of FCA (dashed line) with the absorption bands of Fig. 5.

C. Intraband Free-Carrier Absorption

Free-carrier absorption is a second-order process involving photon absorption and simultaneous scattering by a phonon or lattice defect.[26–30] Quantum mechanically, the FCA process can proceed through two equally probable paths. In the first, a free carrier absorbs a photon and makes a transition to a virtual (but momentum-conserving) intermediate state from which it is then scattered to a final state, conserving both momentum and energy in the over-all process. The second FCA process is the inverse of the first, i.e., phonon emission or absorption followed by photon absorption. For a single isolated band the intermediate states are nearly identical with the initial (or final) states, owing to the extremely small momentum of the photon. This is illustrated in Fig. 7(a). If, however, there are other bands nearby one has the possibility of additional intermediate states[30] as shown in Fig. 7(b). Previous calculations of FCA have been concerned with n-type materials and have utilized the isolated-band approximation quite successfully. In what follows, we shall consider FCA in the valence bands where two or more bands participate.

The model of Fig. 7(b) is directly applicable to semiconductors in which the spin-orbit splitting is large and v_3 is far removed from v_1 and v_2. In the case of GaP, the v_3 band can be ignored as a source of intermediate states only for $\lambda \gg 15$ μ. A correct theory would have to treat simultaneous direct and indirect absorption in all three of the (warped, nonparabolic) valence bands shown in Fig. 3. As a first approximation, however, the idealized two-band model of Fig. 7(b) will be used to calculate the effect of the v_2 and v_3 bands on FCA in v_1 for $\lambda \ll 15$ μ. Thus, we will identify v_1 with v_d and consider v_s to be an average of v_2 and v_3. Both v_d and v_s will be assumed to be isotropic and parabolic with effective masses m_d^* and m_s^*, respectively.

Following Dumke,[30] we write the second-order matrix element for FCA as

$$M = \frac{\langle v_d, \vec{k}_f | \mathcal{H}_{lat} | v_d, \vec{k}_i \rangle \langle v_d, \vec{k}_i | \mathcal{H}_{rad} | v_d, \vec{k}_i \rangle}{-\hbar\omega} + \frac{\langle v_d, \vec{k}_f | \mathcal{H}_{rad} | v_d, \vec{k}_f \rangle \langle v_d, \vec{k}_f | \mathcal{H}_{lat} | v_d, \vec{k}_i \rangle}{\hbar\omega} + \frac{\langle v_d, \vec{k}_f | \mathcal{H}_{lat} | v_s, \vec{k}_i \rangle \langle v_s, \vec{k}_i | \mathcal{H}_{rad} | v_d, \vec{k}_i \rangle}{E_{v_s}(\vec{k}_i) - E_{v_d}(\vec{k}_i) - \hbar\omega} + \frac{\langle v_d, \vec{k}_f | \mathcal{H}_{rad} | v_s, \vec{k}_f \rangle \langle v_s, \vec{k}_f | \mathcal{H}_{lat} | v_d, \vec{k}_i \rangle}{E_{v_s}(\vec{k}_f) - E_{v_d}(\vec{k}_i)}, \quad (6)$$

where $|v, \vec{k}\rangle$ denote Bloch states in band v_d or v_s having initial- or final-state momenta $\vec{k}_i$ or $\vec{k}_f$,

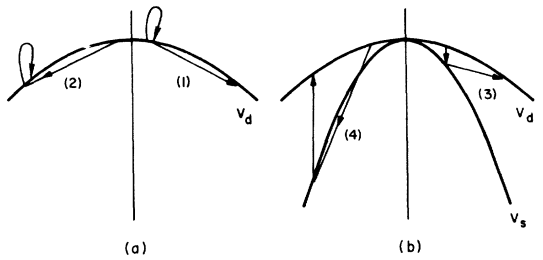

FIG. 7. (a) FCA in an isolated band where momentum conservation demands that the intermediate states be very close to the initial (a) or final (b) states. In (a) the photon is absorbed *before* scattering occurs, and in (b) the absorption occurs *after* scattering. (b) FCA in the case where there are additional intermediate states available in nearby bands. In this case processes (1) – (4) must all be considered simultaneously.

and $\mathcal{H}_{\text{rad}}$ and $\mathcal{H}_{\text{lat}}$ are the Hamiltonians for photon absorption and lattice scattering, respectively. Photon emission is easily accounted for at a later point in the calculation. The first two terms correspond to ordinary intraband FCA proceeding through intermediate states in v_d. The third and fourth terms involve intermediate states in v_s. The energy denominators correspond to the differences between the energies of the intermediate and initial states, and as such, represent the amounts by which the intermediate states fail to conserve energy. We have assumed in Eq. (6) that the phonon energies can be neglected. It should be noted that the denominator of the third term is resonant when $\hbar\omega = E_{v_s}(\vec{k}_i) - E_{v_d}(\vec{k}_i)$. This corresponds to absorption via energy-conserving intermediate states in v_s and requires a theoretical treatment beyond the scope of this paper. We will assume $\hbar\omega \gg E_{v_s}(\vec{k}_i) - E_{v_d}(\vec{k}_i)$ and proceed to calculate the FCA in this high-energy limit.

The Hamiltonian for photon absorption is given by

$$\mathcal{H}_{\text{rad}} = -\frac{e}{nm_0}\left(\frac{2\pi\hbar N}{\omega V}\right)^{1/2} \vec{\xi}\cdot\vec{\mathrm{P}} \,, \tag{7}$$

where m_0 is the free-electron mass, N is the number of photons in a given electromagnetic mode, n is the index of refraction, V is the volume of the crystal, $\vec{\xi}$ is the photon polarization vector, and $\vec{\mathrm{P}}$ is the momentum operator $-i\hbar\vec{\nabla}$. The Hamiltonian for scattering depends on the assumed scattering mechanism. We have recently shown[37] that acoustic and nonpolar optical-phonon scattering appear to be dominant in the p-type III–V semiconductors. For the sake of simplicity, however, we will assume only acoustic-mode scattering in this calculation. Under this assumption $\mathcal{H}_{\text{lat}}$ will be taken to be

$$\mathcal{H}_{\text{lat}} = i\frac{E_{\text{AC}}}{\mu_s}\left(\frac{kT}{2\rho V}\right)^{1/2}\frac{\vec{\xi}\cdot\vec{q}}{|\vec{q}|}\,\delta_{\vec{k}_f-\vec{k}_i,\vec{q}} \,, \tag{8}$$

where E_{AC} is the acoustic-mode deformation potential, μ_s is a suitably averaged sound velocity, ρ is the mass density of the crystal, V is the crystal volume, $\vec{\xi}$ is the phonon polarization vector, and $\vec{q}$ is the phonon wave vector. We have assumed equipartition of energy and linear dispersion in the acoustic modes so that the phonon occupation numbers for emission and absorption can be approximated by $n_q \approx n_q + 1 \approx kT/\hbar\omega_q$ and $\omega_q = |q|u_s$. This is consistent with ignoring the phonon energy $\hbar\omega_q$ in Eq. (6) and allows us to obtain the result for phonon emission *and* absorption by simply doubling the absorption calculated using Eq. (8).

In order to evaluate the matrix elements in Eq. (6) one must expand the hole wave functions at $\vec{k}_i$ in terms of wave functions at $\vec{k}_f$ using $\hbar(\vec{k}_i - \vec{k}_f)\cdot\vec{\mathrm{P}}$ as a perturbation,[30] i.e.,

$$|v,\vec{k}_i\rangle = |v,\vec{k}_f\rangle + \sum_{v'\neq v}\frac{\hbar(\vec{k}_i-\vec{k}_f)\langle v',\vec{k}_f|\vec{\mathrm{P}}|v,\vec{k}_f\rangle}{m_0[E_v(\vec{k}_f)-E_{v'}(\vec{k}_f)]}\,|v',\vec{k}_f\rangle \,, \tag{9}$$

where the sum over v' extends, in principle, over all energy bands $v' \neq v$ in the crystal. We will assume that only the term $v' = v_s$ makes a significant contribution. Using Eqs. (7)–(9) in Eq. (6) and evaluating the intraband matrix elements in the standard way we obtain

$$M = \frac{e}{nm_0}\left(\frac{2\pi\hbar N}{\omega V}\right)\left(\frac{kT}{2\rho V}\right)^{1/2}\frac{E_{\text{AC}}}{u_s}\,\frac{\hbar(\vec{k}_i-\vec{k}_f)\cdot\vec{\xi}}{-\hbar\omega} + \frac{\hbar(\vec{k}_i-\vec{k}_f)}{m_0}\left(\frac{\langle v_d,\vec{k}_f|\vec{\mathrm{P}}|v_s,\vec{k}_f\rangle\langle v_s,\vec{k}_i|\vec{\mathrm{P}}\cdot\vec{\xi}|v_d,\vec{k}_i\rangle}{\Delta_1\Delta_2} + \frac{\langle v_d,\vec{k}_f|\vec{\mathrm{P}}\cdot\vec{\xi}|v_s,\vec{k}_f\rangle\langle v_s,\vec{k}_f|\vec{\mathrm{P}}|v_d,\vec{k}_f\rangle}{\Delta_1\Delta_3}\right) \,, \tag{10}$$

where

$$\Delta_1 = \Delta_0 + \frac{\hbar^2k_f^2}{2m_s^*} - \frac{\hbar^2k_f^2}{2m_d^*} \,,$$
$$\Delta_2 = \Delta_0 + \frac{\hbar^2k_i^2}{2m_s^*} - \frac{\hbar^2k_i^2}{2m_d^*} - \hbar\omega \,, \tag{11}$$

and

$$\Delta_3 = \Delta_0 + \frac{\hbar^2k_f^2}{2m_s^*} - \frac{\hbar^2k_i^2}{2m_d^*} \,.$$

The interband momentum matrix elements will be approximated as follows. In crystals with inversion symmetry the intervalence-band momentum matrix elements vanish at $k = 0$.[24] Since GaP lacks inversion symmetry, the matrix elements are not required to vanish but they should, nonetheless, be quite small near $k = 0$. We will therefore write

$$\langle v_s,\vec{k}_i|\vec{\mathrm{P}}|v_d,\vec{k}_i\rangle = A\hbar\vec{k}_i \,,$$
$$\langle v_s,\vec{k}_f|\vec{\mathrm{P}}|v_d,\vec{k}_f\rangle = B\hbar\vec{k}_f \,, \tag{12}$$

where A and B are dimensionless parameters.

With the help of Eq. (12) we obtain the following for $|M|^2$:

$$|M|^2 = \frac{2\pi NkT}{\rho(\hbar\omega)^3}\left(\frac{e\hbar^2 E_{AC}}{nm_d^* V u_s}\right)\{(\vec{k}_i - \vec{k}_f)\cdot\vec{\xi} + \mathcal{L}_1[(\vec{k}_i - \vec{k}_f)\cdot\vec{k}_f](\vec{k}_f\cdot\vec{\xi}) - \mathcal{L}_2[(\vec{k}_i - \vec{k}_f)\cdot\vec{k}_f](\vec{k}_i\cdot\vec{\xi})\}^2 , \quad (13)$$

where

$$\mathcal{L}_1 = \hbar^3\omega AA^* m_d^*/m_0^2\Delta_1\Delta_3 \quad (14)$$

and

$$\mathcal{L}_2 = \hbar^3\omega AB m_d^*/m_0^2\Delta_1\Delta_2 . \quad (15)$$

The factor of 2 in Eq. (13) takes account of the fact that phonon emission and absorption contribute equally. The square of the transition matrix element can be related to the absorption coefficient, α, by

$$\alpha = -\frac{n}{c}\frac{1}{N}\frac{dN}{dt} \quad (16)$$

or

$$\alpha = (n/c)(1/N)(pV)(1 - e^{-\hbar\omega/kT})\int\int \mathcal{P}(\vec{k}_i, \vec{k}_f) f_{\vec{k}_i} \times (2V/8\pi^3)^2 d^3k_i d^3k_f , \quad (17)$$

where p is the hole concentration, $f_{\vec{k}_i}$ is the classical Maxwell-Boltzmann distribution function

$$f_{\vec{k}_i} = \frac{(2\pi)^3}{2V}\left(\frac{\hbar^3}{2\pi m_d^* kT}\right)^{3/2}\exp\left(-\frac{\hbar^2 k_i^2}{2m_d^* kT}\right) , \quad (18)$$

and $\mathcal{P}(\vec{k}_i, \vec{k}_f)$ is the transition rate given by Fermi's golden rule

$$\mathcal{P}(\vec{k}_i, \vec{k}_f) = (2\pi/\hbar)\langle|M|^2\rangle\,\delta[E_{v_d}(\vec{k}_f) - E_{v_d}(\vec{k}_i) - \hbar\omega] . \quad (19)$$

In Eq. (19), $\langle\cdots\rangle$ indicates an average over all polarization directions $\vec{\xi}$. In order to evaluate α we make the following approximations:

$$\Delta_1 \approx \hbar^2 k_f^2/2m_r^* , \quad \Delta_2 \approx -\hbar\omega , \quad \Delta_3 \approx \hbar^2 k_f^2/2m_s^* , \quad (20)$$

where

$$1/m_r^* = 1/m_s^* - 1/m_d^* . \quad (21)$$

With these approximations, the integrals in Eq. (17) become tractable. It can be shown (see Appendix A) that the absorption coefficient can be written in terms of the modified Bessel functions K_0, K_1, and K_2 as follows:

$$\alpha = \alpha_0\left\{E\frac{\sinh X K_2(X)}{X} + F\frac{\sinh X K_1(X)}{X} + G\sinh X[K_1(X) - K_0(X)]\right\} , \quad (22)$$

where $X = \hbar\omega/2kT$ and α_0 is given by

$$\alpha_0 = p\,\frac{8e^2}{3\hbar^2 c}\left(\frac{2}{\pi kT}\right)^{1/2}\frac{(m_d^*)^{1/2}E_{AC}^2}{n\rho u_s^2} . \quad (23)$$

In the limit in which transitions through intermediate states in v_s are forbidden, the coefficients in Eq. (22) are $E = 1$, $F = G = 0$. This leads to precisely the result obtained by Rosenberg and Lax[27] and Meyer[28] for FCA in isolated bands. [Their equations apply to ellipsoidal energy surfaces and must be reduced to the case of an isotropic band of mass m_d^* for comparison with Eq. (22).] In the high-energy limit ($X \gg 1$) the three terms in Eq. (22) have nearly identical wavelength dependences (see Appendix B) and α is given approximately by

$$\alpha \approx \tfrac{1}{2}\alpha_0(\tfrac{1}{2}\pi)^{1/2}X^{-3/2}[1 + \tfrac{1}{3}(3S_1^2 + 6S_1 - 8S_2)] , \quad (24)$$

where

$$S_1 = 2(m_r^* m_s^*/m_0^2)AA^* \quad (25)$$

and

$$S_2 = 2(m_r^* m_d^*/m_0^2)AB . \quad (26)$$

Within the framework of the present model, we conclude from Eq. (22) that the principal effect of the v_2 and v_3 bands on FCA in the v_1 band is an enhancement of the *magnitude* of the absorption without a significant alteration of the wavelength dependence. We now discuss the extent to which this conclusion depends on specific approximations of our model. We have assumed that the valence bands of GaP (Fig. 3) can be approximated by the model shown in Fig. 7(b) in which the v_2 and v_3 bands are replaced by an average band v_s which, along with v_d, is assumed to be isotropic and parabolic. In a more realistic three-band model Eq. (6) would have additional terms corresponding to transitions involving the third band. This would cause a considerable increase in the complexity of Eq. (13) but the new terms would still lead to integrals of the form discussed in Appendix A and would not generate any radically new wavelength dependence. Thus, removal of the artifice of v_s would lead to severe complications in the calculation without adding any qualitatively new features. The assumption of isotropic, parabolic bands is quite reasonable if one uses suitably averaged effective masses for v_s and v_d. In order to avoid resonant energy denominators and as an aid in evaluating the integrals of Eq. (17) we have worked in the high-energy limit by using the approximations given in Eq. (20). Strictly speaking, this restricts the validity of our calculation to wavelengths $\lambda \lesssim 3$–$4\ \mu$ (for GaP). The use of the high-energy approximations may be less restrictive than this, however, since the physical process which leads to the res-

onant denominators corresponds to a direct (allowed) transition from v_d to v_s followed by a scattering from v_s to v_d. This process is likely to be quite similar to the $v_1 \rightarrow v_3$ interband absorption discussed above in Sec. III B and, to that extent, does not contribute to a Drude-like background. The approximation used for the momentum matrix elements [Eq. (12)] is standard. Although it is possible that a correct treatment of these matrix elements would alter the wavelength dependence of α, a more refined treatment depends on details of the valence-band wave functions and is not justified in the context of our present model. Finally, we have assumed for simplicity only acoustic-mode deformation-potential scattering. Although we have not carried out calculations for other scattering mechanisms, they should proceed along similar lines and their characteristic wavelength dependences should be preserved. As has been mentioned above, the characteristic wavelength dependence for FCA due to acoustic and NPO scattering is $\lambda^{1.7}$. This is consistent with the background absorption for which we obtain agreement between theory and experiment. Although reasonable fits to the data can be obtained with $\alpha_{FCA} \propto \lambda^p$, where $1.5 < p < 2$, the data are definitely inconsistent with a p value as large as 2.5 (polar-mode scattering).

III. ABSORPTION AT 90°K

In Fig. 8, we show the absorption of samples B, C, and D at 90 °K. We estimate that at this temperature the Zn acceptors are only 2–3% ionized so that the absorption is almost entirely due to photoionization.[42] The threshold for the onset of transitions from the acceptor levels to v_1 and v_2 is at $\hbar\omega = E_A$, where E_A is the Zn ionization energy. For sample B, $E_A \approx 60$ meV [32] and the threshold occurs at $\lambda \approx 21$ μ. For samples C and D, E_A is smaller and the threshold is at longer wavelengths (further into the lattice absorption). The structure in the 8–9-μ region is associated with the onset of transitions from the acceptors to the splitoff valence band. This process has a threshold of $\hbar\omega = E_A + \Delta_0$ and should be expected to occur for $\lambda \lesssim 9$ μ. Aside from the sharper threshold for transitions to the splitoff valence band, and a slightly stronger overall absorption cross section, the general appearance of the low-temperature absorption is quite similar to that at 300 °K. This permits two related observations concerning the Zn acceptor levels: (i) The k-space extent of the acceptors is comparable to the 300 °K thermal occupation of the valence bands ($k \approx 0.05 a_0^{-1}$ corresponds to $E \approx kT$ for v_1 at 300 °K), and (ii) the Zn levels cannot be classified as being either "shallow" (purely Coulombic) or "deep" (dominated by the core potential). The latter observation is based on the $\lambda^{1.8}$ wavelength dependence of the high-energy tail of the photoionization absorption. The hydrogenic model for shallow acceptors predicts a $\lambda^{3.5}$ dependence and Lucovsky's model[43] for deep levels predicts a $\lambda^{1.5}$ dependence. Using the quantum-defect method, Bebb[44] has shown that the shape of the photoionization absorption passes smoothly from the "deep" limit of Lucovsky's δ-function core potential to the "shallow" limit of a pure Coulomb potential.

The strength of the photoionization absorption and its qualitative similarity to the room-temperature absorption places an important practical restraint on the study of other IR absorption processes in Zn-doped GaP. Any process which is masked by strong absorption at 300 °K will be even further masked by photoionization absorption at low temperatures for $\lambda \lesssim 20$–25 μ.

IV. SUMMARY AND CONCLUSIONS

Because of the complexity of the valence bands, infrared absorption in p-type semiconductors usually contains a wealth of structure associated with direct interband transitions. We have shown experimentally that the 300 °K absorption in p-type GaP displays very little structure and that the explanation for this is twofold. First, estimates of the α_{12}, α_{13}, and α_{23} absorption bands (based on a $\vec{k} \cdot \vec{p}$ calculation of the valence-band structure) show that these absorption bands in GaP are broad and overlapping rather

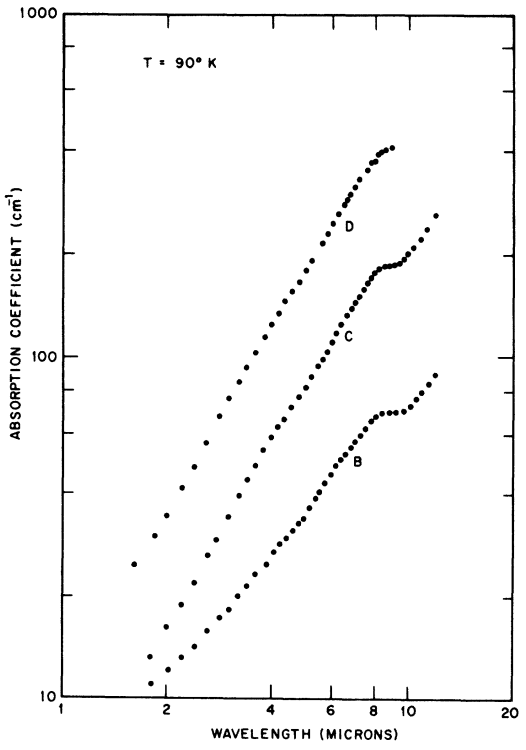

FIG. 8. Experimental absorption data for samples B, C, and D at 90 °K.

than sharp and well separated as in Ge or GaAs. Second, we have shown that the close proximity of the splitoff valence band can lead to an enhancement of the intraband FCA in the upper valence band. This effect is difficult to calculate in general but an enhancement of a factor of 4 over the Drude theory would be sufficient to explain our results. We conclude that the room-temperature absorption data are best fit by a combination of direct interband absorption and a $\lambda^{1.7}$ Drudelike background of FCA. The wavelength dependence of the FCA is indicative of acoustic and nonpolar optical-mode scattering. Any contribution from polar-mode scattering must be considerably weaker since the predicted wavelength dependence for FCA in the case of polar-mode scattering is $\lambda^{2.5}$ and this is much too steep to fit the data over our experimental wavelength range.

The absorption at low temperatures is identified as arising from the photoionization of holes from the Zn acceptor levels to the valence bands. The threshold for transitions to the v_1 and v_2 bands lies in the region of strongest lattice absorption and is hence experimentally inaccessible. The threshold for transitions to the splitoff valence band is observed in the $8-10-\mu$ region and is consistent with the spin-orbit splitting $\Delta_0 = 82$ meV as measured by Dean *et al.*[21] and Zn ionization energies of $E_A \leq 60$ meV as reported by Casey *et al.*[32]

ACKNOWLEDGMENTS

It is a pleasure to acknowledge several valuable discussions with R. A. Faulkner during the course of this work. We have also benefitted from discussions with M. Lax. Technical assistance was very ably provided by J. A. Seman. The crystals were grown by L. Derick.

APPENDIX A

After averaging over the polarization directions $\vec{\xi}$, the integral in Eq. (17) reduces to a set of integrals of the form

$$I = \int d\vec{k}_i \int d\vec{k}_f \, k_i^m \, k_f^n \, g(\theta) \exp\left(-\frac{\hbar^2 k_i^2}{2m_d^* kT}\right) \times \delta\left(\frac{\hbar^2 k_f^2}{2m_d^*} - \frac{\hbar^2 k_i^2}{2m_d^*} - \hbar\omega\right) , \tag{A1}$$

where m and n are integers and $g(\theta)$ is a function of the angle θ between k_i and k_f. In each case the angular integration is trivial so we will consider only the k_i and k_f integrations:

$$J = \int_0^\infty k_i^2 \, dk_i \int_0^\infty k_f^2 \, dk_f \, k_i^m \, k_f^n \exp\left(-\frac{\hbar^2 k_i^2}{2m_d^* kT}\right) \times \left(\frac{2m_d^*}{\hbar^2}\right) \delta\left[k_f^2 - \left(k_i^2 - \frac{2m_d^* \omega}{\hbar}\right)\right] . \tag{A2}$$

Letting $\epsilon = k_f^2$ and integrating over ϵ yields

$$J = \frac{1}{2}\left(\frac{2m_d^*}{\hbar^2}\right) \int_0^\infty k_i^{m+2} \left(k_i^2 + \frac{2m_d^* \omega}{\hbar}\right)^{(n+2)/2} \times \exp\left(-\frac{\hbar^2 k_i^2}{2m_d^* kT}\right) dk_i . \tag{A3}$$

If we now perform the transformation

$$k_i^2 = (2m_1^* \omega/\hbar) \sinh(\tfrac{1}{2}\theta) , \tag{A4}$$

then J becomes

$$J = \left(\frac{2m_d^*}{\hbar^2}\right)^{(m+n+6)/2} (\hbar\omega)^{(m+n+4)/2} \left(\tfrac{1}{2}\right)^{(m+n+8)/2} e^X \times \int_0^\infty (\cosh\theta - 1)^{(m+2)/2} \, (\cosh\theta + 1)^{(n+2)/2} \times e^{-X\cosh\theta} \, d\theta . \tag{A5}$$

This result, when combined with the integral representation of the modified Bessel function[45]

$$K_n(X) = \int_0^\infty \cosh n\theta \, e^{-X\cosh\theta} \, d\theta , \tag{A6}$$

enables one to evaluate the integrals encountered in Eq. (17). In reducing the resulting expressions to the form given in Eq. (22) the following properties of the $K_n(X)$ Bessel functions are useful[45]:

$$K_3(X) - K_1(X) = 4K_2(X)/X \tag{A7}$$

and

$$K_2(X) - K_0(X) = 2K_1(X)/X .$$

Using the definitions of S_1 and S_2 given in Eqs. (25) and (26), the coefficients E, F, and G of Eq. (22) are given by

$$E = 1 + \tfrac{2}{3} S_2^2 - \tfrac{4}{3} S_2 ,$$

$$F = \tfrac{1}{3}[4(2S_1 - S_2) + (2S_1 - S_2)^2 - 3S_1^2 - 4S_2^2] , \tag{A8}$$

$$G = \tfrac{2}{3}[(2S_1 + S_2)^2 - 2S_1(1 + S_1)] .$$

APPENDIX B

In the limit $X \gg 1$, the modified Bessel functions can be approximated by the asymptotic expansion[45]

$$K_n(X) \sim (\pi/2X)^{1/2} e^{-X} [1 + (4n^2 - 1)/8X + \cdots] . \tag{B1}$$

In this limit, the terms of Eq. (22) become

$$K_1(X)/X \approx K_2(X)/X \sim e^{-X}(\pi/2X)^{1/2}(1/X) , \tag{B2}$$

$$K_1(X) - K_0(X) \sim e^{-X}(\pi/2X)^{1/2}(1/2X) . \tag{B3}$$

These approximations, together with $\sinh X \approx e^X/2$, lead to Eq. (24).

[1]For references to early work on Ge and Si, see E. Burstein, G. Picus, and N. Sclar, in *Photoconductivity Conference*, edited by R. G. Breckenridge, B. R. Russell, and E. E. Hahn (Wiley, New York, 1956).
[2]W. G. Spitzer and J. M. Whelan, Phys. Rev. 114, 59 (1959).
[3]M. D. Sturge, Phys. Rev. 127, 768 (1962).
[4]I. Balslev, Phys. Rev. 173, 762 (1968).
[5]R. Braunstein and E. O. Kane, J. Phys. Chem. Solids 23, 1423 (1962).
[6]I. Balslev, Phys. Rev. 177, 1173 (1969).
[7]W. Cochran, S. J. Fray, F. A. Johnson, J. E. Quarrington, and N. Williams, J. Appl. Phys. 32, 2102 (1961).
[8]W. G. Spitzer, J. Appl. Phys. 34, 792 (1963).
[9]E. Haga and H. Kimura, J. Phys. Soc. Japan 18, 777 (1963); 19, 471 (1964); 19, 658 (1964).
[10]E. Haga, J. Phys. Soc. Japan 19, 2030 (1964); 20, 735 (1965).
[11]S. Perkowitz, J. Appl. Phys. 40, 3751 (1969).
[12]J. W. Allen and J. W. Hodby, Proc. Phys. Soc. (London) 82, 315 (1963).
[13]J. W. Hodby, Proc. Phys. Soc. (London) 82, 324 (1963).
[14]K. Osamura and Y. Murakami, J. Phys. Soc. Japan 26, 1063 (1969).
[15]Y. S. Chen, W. Shockley, and G. L. Pearson, Phys. Rev. 151, 648 (1966).
[16]W. G. Spitzer, M. Gershenzon, C. J. Frosch, and D. F. Gibbs, J. Phys. Chem. Solids 11, 339 (1959).
[17]W. Paul, J. Appl. Phys. 32, 2082 (1961).
[18]R. Zallen and W. Paul, Phys. Rev. 134, A1628 (1964).
[19]A. D. Remenyuk, L. G. Zabelina, Yu. I. Uklianov, and Yu. V. Shmartsev, Fiz. Tekh. Poluprov. 2, 666 (1968); 2, 671 (1968) [Soviet Phys. Semicond. 2, 557 (1968); 2, 561 (1968)].
[20]J. D. Wiley and M. DiDomenico, Jr., Phys. Rev. B 1, 1655 (1970).
[21]P. J. Dean, G. Kaminsky, and R. B. Zetterstrom, J. Appl. Phys. 38, 3551 (1967).
[22]D. A. Kleinman and W. G. Spitzer, Phys. Rev. 118, 110 (1960).
[23]A. S. Barker, Jr., Phys. Rev. 165, 917 (1968).
[24]A. H. Kahn, Phys. Rev. 97, 1647 (1955).
[25]E. O. Kane, J. Phys. Chem. Solids 1, 82 (1956).
[26]H. Y. Fan, W. Spitzer, and R. S. Collins, Phys. Rev. 101, 566 (1956).
[27]R. Rosenberg and M. Lax, Phys. Rev. 112, 843 (1958).
[28]H. J. G. Meyer, Phys. Rev. 112, 298 (1958).
[29]S. Visvanathan, Phys. Rev. 120, 376 (1960); 120, 379 (1960).
[30]W. Dumke, Phys. Rev. 124, 1813 (1961).
[31]L. M. Foster and J. Scardefield, J. Electrochem. Soc. 116, 494 (1969). Also see J. M. Dishman, M.. DiDomenico, Jr., and R. Caruso, Phys. Rev. B 2, 1988 (1970).
[32]H. C. Casey, F. Ermanis, and K. B. Wolfstirn, J. Appl. Phys. 40, 2945 (1968).
[33]J. S. Blakemore, *Semiconductor Statistics* (Pergamon, London, 1962).
[34]T. S. Moss, *Optical Properties of Semiconductors* (Butterworth, London, 1961).
[35]W. L. Bond, J. Appl. Phys. 36, 1674 (1965).
[36]A. S. Barker (private communication).
[37]J. D. Wiley and M. DiDomenico, Jr., Phys. Rev. B 2, 427 (1970).
[38]R. A. Faulkner (private communication). These parameters were calculated by Faulkner using the pseudopotentials of M. L. Cohen and T. K. Bergstresser, Phys. Rev. 141, 789 (1966).
[39]R. L. Bowers and G. D. Mahan, Phys. Rev. 185, 1073 (1969).
[40]O. G. Lorimor, J. Appl. Phys. 41, 5035 (1970).
[41]J. M. Dishman and M. DiDomenico, Jr. (unpublished).
[42]The anomalous wavelength dependence of sample *B* at short wavelengths is not understood but was present in two samples of the same material.
[43]G. Lucovsky, Solid State Commun. 3, 299 (1965).
[44]H. B. Bebb and R. A. Chapman, J. Phys. Chem. Solids 28, 2087 (1967); H. B. Bebb, Phys. Rev. 185, 1116 (1969).
[45]*Handbook of Mathematical Functions*, edited by M. Abramowitz and I. A. Stegun (U. S. GPO, Washington, D. C., 1964).

PHYSICAL REVIEW B VOLUME 3, NUMBER 2 15 JANUARY 1971

Phonon Conductivity of II-VI Semiconductors

K. C. Sood, M. P. Singh, and G. S. Verma
Physics Department, Banaras Hindu University, Varanasi-5, India
(Received 22 July 1970)

It is shown in the present work that the change in the slope of K-vs-T curve, which occurs in CdS and CdTe at a temperature beyond the conductivity maximum, can be explained by considering the separate contributions of longitudinal phonons and transverse phonons. The values of the limits of the different conductivity integrals for the different acoustic branches are taken from the theoretical work of Nusimovici and Birman for CdS and from Hayes's work for CdTe. The present work also establishes that transverse phonons make a major contribution towards phonon conductivity.

I. INTRODUCTION

It is now well established that in several semiconductors there occurs a change in the slope of K-vs-T curve in the high-temperature region and that this cannot be explained by one conductivity integral as given in Callaway's[1] theory of phonon conductivity. The well-known examples are Si and Ge.[2] Holland[2] explained the high-temperature re-